Environmental Science Nano

PAPER

Cite this: *Environ. Sci.: Nano*, 2016, 3, 1504

# Electrochemical DNA sensing strategy based on strengthening electronic conduction and a signal amplifier carrier of nanoAu/MCN composited nanomaterials for sensitive lead detection†

Guangming Zeng,*[ab] Yuan Zhu,[ab] Yi Zhang,*[ab] Chang Zhang,[ab] Lin Tang,[ab] Pucan Guo,[ab] Lihua Zhang,[ab] Yujie Yuan,[ab] Min Cheng[ab] and Chunping Yang[ab]

Received 9th August 2016,
Accepted 7th November 2016

DOI: 10.1039/c6en00323k

rsc.li/es-nano

A DNA electrochemical sensor was fabricated using the modification of a glassy carbon electrode (GCE) with ordered mesoporous carbon nitride (MCN), electrodeposited gold nanoparticles (EAu) and methylene blue (MB)/nanoAu/MCN as the signal amplifier, in which MB was inserted into the nanoAu/MCN composites for $Pb^{2+}$ detection. The secondary structure of the *trans*-cleaving 8–17 DNAzyme, composed of the substrate strand (S1) and the enzyme strand (S2), was utilized for the sensor fabrication. S1 immobilized on the signal amplifier could hybridize with S2 and form a DNA double helix structure on account of the principle of complementary base pairing. With the activation of $Pb^{2+}$, S2 was able to cleave the single RNA linkage with S1 by hydrolysis reaction to break S1 into two fragments. One of the fragments NS1′ that was immobilized on the MB/nanoAu/MCN signal amplifier (S1′/MB/nanoAu/MCN) could hybridize with the DNA probe S3 immobilized on the modified electrode. With the help of the MCN's large specific surface area and the gold nanoparticles' good charge-transport capacity, the sensor exhibited excellent sensitivity and selectivity. The proposed sensing strategy represented a wide linear response in the range from $1.0 \times 10^{-3}$ to $1.0 \times 10^{-14}$ M. The sensor was also tested with real samples and represented a promising method for detecting $Pb^{2+}$.

**Environmental significance**

MCN and electrodeposited gold nanoparticles were utilized to enhance the electrical conductivity in the sensor. The electrical signal was amplified by MB/nanoAu/MCN in the detection process. And the biosensor has potential applications in detecting $Pb^{2+}$ in water samples.

## 1. Introduction

Heavy metals (*e.g.* lead, mercury, cadmium, chromium *etc.*) cannot be biodegraded, and can be enriched in the environment and human bodies.[1–3] Lead (Pb) can cause serious physical injuries, especially nervous system damage.[4,5] Therefore, the accurate detection of $Pb^{2+}$ is of significance in the environment[6] and food tracking,[7] as well as clinical toxicology.[7] Traditional lead determination methods have been used, such as atomic absorption spectrometry,[8] ion chromatography[9] and spectrophotometry,[10] *etc.* However, compared with those analytical means, the sensing strategy is more convenient as it does not need expensive and huge instruments or complicated sample preparation processes.[11,12]

Many efforts have been devoted toward the design of electrochemical sensors for $Pb^{2+}$ determination in past decades.[13,14] Alternatively, DNA sensors are a very important and attractive method. It has been reported that DNA and RNA possess the ability to catalyze numerous biological reactions in the presence of metal ions following the activity order of $Pb^{2+} \gg Zn^{2+} \gg Mg^{2+}$.[15] A $Pb^{2+}$-dependent RNA-cleaving DNAzyme probe has been utilized in sensors for $Pb^{2+}$ detection.[16] The secondary structure of 8–17 DNAzyme is a DNA metalloenzyme, which can catalyze RNA transesterification with the existence of $Pb^{2+}$, and the DNAzyme substrate strand can split at the single RNA linkage due to the hydrolysis reaction catalyzed by the enzyme strand. This property of the probe can ensure the selectivity of the electrochemical sensor in $Pb^{2+}$ determination.[17,18]

[a] *College of Environmental Science and Engineering, Hunan University, Changsha 410082, PR China. E-mail: zgming@hnu.edu.cn, zyi@hnu.edu.cn; Fax: +86 731 88823701; Tel: +86 731 88822754*
[b] *Key Laboratory of Environmental Biology and Pollution Control (Hunan University), Ministry of Education, Changsha 410082, PR China*

† Electronic supplementary information (ESI) available. See DOI: 10.1039/c6en00323k

With the development of science and technology, more and more nano-materials have been synthesized and applied in sensing strategies.[19,20] Carbon materials, like carbon nanotubes[21,22] and graphene,[23,24] have been widely used in the sensing field. In addition, ordered mesoporous carbon (OMC), as a good candidate, is a favorable material for fabricating sensors.[25,26] OMC has the fantastic characteristics of tremendous specific surface area and pore volume, favorable biocompatibility and excellent corrosion resistance.[28] The most important reasons for the OMC utilization in electrochemical sensing are that OMC has the ability to ameliorate the electrical conductivity and provide more active sites for nanoparticles or bioactive materials.[27] Moreover, nitride-doped mesoporous carbon, a derivative of OMC, possesses better electrical conductivity. Ordered mesoporous carbon nitride (MCN) can be easily synthesized by environmentally friendly methods, *e.g.* block copolymer methods with much better electrical conductivity than that prepared with particles bonding together. The resistance of MCN consists of two parts: one is the intraparticle resistance, the other is the interparticle resistance, and the latter's role is greater. However, MCN that is synthesized with the method of block copolymers calcining has lower interparticle resistance and better electrical conductivity. Obviously, the above characteristics inspire us to apply MCN to fabricate a highly sensitive sensor. In addition, MCN can notably disperse nanoparticles and is a desirable carrier due to its extremely huge specific surface area and pore volume. Similarly, gold nanoparticles possess good specific surface area and electrical conductivity, and can combine with a variety of biological molecules and keep the biological activity.[28,29] The nanoscale Au is modified on the MCN to obtain the composite materials, which can enhance the electrical conductivity and improve the electrochemical response in the electrochemical sensor for $Pb^{2+}$ detection.

Herein, we fabricated a DNA electrochemical sensor to cover the $Pb^{2+}$ determination concentrations of 13 orders of magnitude. The result exhibited that the enhancement of electrical conductivity was primarily attributed to the MCN and electrodeposited gold particle (EAu) modified electrode and MB was immobilized on the nanoAu/MCN composite materials under the optimized conditions as the signal amplifier. Moreover, the 8–17 DNAzyme was beneficial to the selectivity of the DNA electrochemical sensor.

# 2. Experimental section

### 2.1. Materials and apparatus

Lead nitrate, methylene blue, *N*,*N*-dimethylformamide (DMF) and 6-mercapto-1-hexanol (MCH) were supplied by Sigma-Aldrich Chemical Co. Hydrochloroauric acid ($HAuCl_4 \cdot 3H_2O$, 99.9%), trisodium citrate and sodium borohydride were purchased from Sinopharm Chemical Reagent Co., Ltd. (Shanghai, China). All other chemicals were of analytical grade. Phosphate buffer solutions (PBS), mixed with $NaH_2PO_4 \cdot 2H_2O$ and $Na_2HPO_4 \cdot 12H_2O$, were used as the probe storage solution. Tris-HCl buffer (10 mM Tris with 1.0 M KCl, pH 8.0) was prepared as the stock solution; Tris-HCl buffer (10 mM Tris with 1.0 M KCl, pH 7.4) was prepared as the supporting electrolyte. Ultrapure water (18.2 MΩ $cm^{-1}$) was used in all runs. DNA stock solution was prepared by dissolving the oligonucleotides in Tris-HCl buffer (pH 8.0). The synthesized oligonucleotides were bought from Sangon Biotech. Co., Ltd. (Shanghai, China), and their sequences were as follows:

S1 (substrate strand): 5′-$NH_2$-TTTACTCACTAT *rA* GGAAGAGATG-T8-HS-3′

S2 (enzyme strand): 5′-CATCTCTTCTCCGAGCCGGTCGAA-ATAGTGAGT-3′

S3: 5′-HS-ATAGTGAGTAAA-3′

Oligonucleotides were heated to 90 °C for 5 min and then cooled down to room temperature at a slow rate before use, and they were preserved at −20 °C for further use.

Electrochemical measurements were conducted on a PGSTAT 302F electrochemistry system (Metrohm, Switzerland). In this work, the three-electrode system consisted of a glassy carbon electrode (GCE, 5 mm in diameter) as the working electrode, a saturated calomel electrode (SCE) as the reference electrode and a Pt foil auxiliary electrode. Scanning electron microscopy (SEM) was performed on a JSM-6360LV scanning electron microscope (JEOL Ltd, Japan). Transmission electron microscopy (TEM) images were obtained using a JEOL-1230 electron microscope (JEOL, Japan) at 100 kV. A Sigma 4K15 laboratory centrifuge (Sigma, Germany) was used in the assay. All experiments were run at room temperature (25 °C) unless otherwise specified.

### 2.2. Preparation of MCN and nanoAu/MCN composite materials

The synthesis of the MCN was similar to our previous work.[30] To obtain the nanoAu/MCN nanocomposites, 0.1 g MCN was dispersed in the mixture solution which contained 9.2 mL ultrapure water, 0.25 mL $HAuCl_4$ (0.01 M) and 0.25 mL trisodium citrate solution (0.01 M). Then 0.3 mL ice cold aqueous sodium borohydride solution (0.1 M) was added to the above mentioned solution with stirring. That solution turned into a wine-red color and was placed in darkness for 3 h. The black solid powder was washed with ultrapure water and dried at 35 °C. The prepared nanocomposites were kept for further experiments.

### 2.3. Sensor fabrication

The MCN was dissolved into 2 mL DMF with sonication for 1 h. The GCE was gently polished with alumina powder of different sizes on buckskin, rinsed thoroughly with acetone and ultrapure water and then air dried. First of all, 7 μL MCN suspension solution was dropped onto the smooth surface of GCE. GCE was washed with ultrapure water to remove excess MCN and dried in the air. Secondly, the modified GCE was immersed into 5 mL 1%(wt) $HAuCl_4$ mixed with 200 μL perchloric acid for electro-deposition at 0.2 V for 60 s, then treated with $H_2SO_4$, and dried for future use. Lastly, 1 μM S3 achieved self-assembly on the EAu/MCN/GCE electrode after

12 h, and then 1 mM MCH was dropped on the electrode and kept at room temperature for 30 min. The modified electrode was preserved in a moist state at 4 °C. Herein, the thiol modified S3 was immobilized on the electrode, then the electrode was treated with MCH to block the excess Au binding sites on its surface based on thiol–gold bonding to prevent the nonspecific binding of other DNA probes. Moreover, MCH can form a dense sublayer on the electrode surface and keep the DNA S3 upright, which facilitates the subsequent hybridization between S3 and NS1′.

### 2.4. Preparation of MB/nanoAu/MCN signal amplifier

0.003 g nanoAu/MCN was dispersed in 50 mL 5.0 mg $L^{-1}$ MB solution (pH 8.0) with stirring at 25 °C, then centrifuged and dried. 50 μL of 2 μM S1 was self-assembled on the MB/nanoAu/MCN (0.5 mg $mL^{-1}$, 10 μL) composites *via* –SH and $–NH_2$. The mixture solution was incubated for 12 h at 4 °C with gentle vibration. Then the mixture solution was re-suspended in 50 μL of stock solution after centrifugation at 4 °C. 20 μL of 2 μM S2 was added into an equivoluminal S1/MB/nanoAu/MCN solution for hybridization at 40 °C for 1 h. The hybridized DNAs reacted with various concentrations of $Pb^{2+}$ in 10 mM Tris buffer with 1.0 M KCl, (pH 8.0) for 30 min at 46 °C for hydrolysis. S2 was activated when $Pb^{2+}$ was added into the solution, then the substrate strand was cleaved, and the hydrolytic cleavage of S1 occured at the scissile *rA* at 46 °C. The S1 split into two parts and S2 was released. And the two parts (NS1′ and SS1′) of S1 still combined on the signal amplifier. NS1′ on the amplifier could hybridize with S3 immobilized on the EAu/MCN modified electrode.

### 2.5. Detection of $Pb^{2+}$

NS1′/MB/nanoAu/MCN was dropped onto the surface of the EAu/MCN/GCE electrode and they hybridized with each other at 40 °C for 1 h. Differential pulse voltammetry (DPV) was utilized for $Pb^{2+}$ detection with the conditions of potential from −0.35 V to −0.75 V, pulse amplitude 0.05 V, pulse width 0.05 s and pulse period 0.2 s.

## 3. Results and discussion

### 3.1. Particle characterization and stability

Scheme 1 shows the sensing strategy. The signal amplifier consisting of MB/nanoAu/MCN was combined with S1 *via* –SH and $–NH_2$. MB was loaded in the pores of MCN and on the MCN surface, which could provide a more adequate electrochemical response signal compared with when it was directly labeled in DNA probes. The secondary structure of 8–17 DNAzyme containing S1 and S2 was chosen in the signal simplifier strategy. S1 was a DNA/RNA chimera including a ribonucleotide adenosine (*rA*), and could hybridize with S2 to form a DNA double helix structure. Because the DNA and RNA had the ability to catalyze the hydrolysis reaction in the presence of $Pb^{2+}$ to activate S2, the DNA double helix structure was unwound and S2 was released. At the same time, S1 was hydrolyzed and cleaved into two fragments at the scissile *rA*. Two fragments of S1, *i.e.* NS1′ and SS1′ respectively representing an amino-modified DNA fragment and a thiol-modified DNA fragment, still combined on the signal simplifier and the NS1′/MB/nanoAu/MCN was obtained *via* –SH and $–NH_2$, respectively. S3 bound on the surface of the EAu/MCN electrode *via* –SH could hybridize with NS1′, and then MB/nanoAu/MCN was connected to the electrode and caused the electrochemical signal amplification. The design of the sensing strategy can give support to specifically distinguishing $Pb^{2+}$.

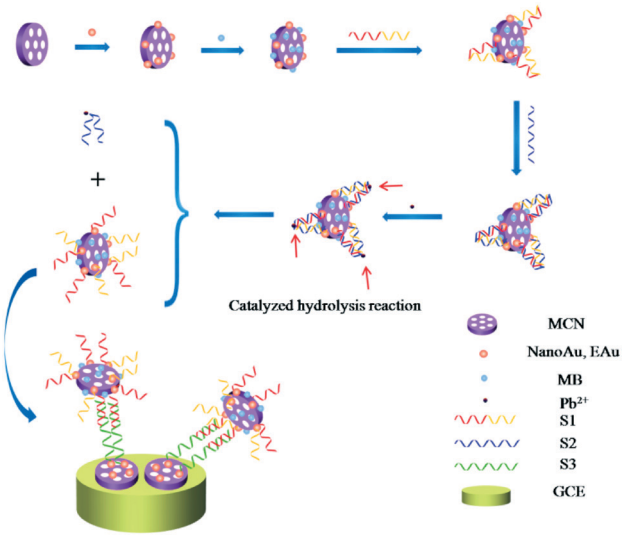


**Scheme 1** Assembly and hybridization of the $Pb^{2+}$ sensor.

### 3.2. Characterization of the MCN, EAu and nanoAu/MCN

To characterize the morphologies of the mentioned materials including the original MCN, EAu/MCN, and nanoAu/MCN, the SEM and TEM images were obtained. It can be observed that the original MCN has a typically ordered mesoporous carbon morphology in TEM and its surface is relatively smooth *via* the high magnification SEM (Fig. S1A†). When EAu was electrodeposited on the MCN modified electrode, the surface of EAu/MCN becomes grainy. The EAu deposited on the MCN surface aggregated in block-shapes with a mean size of ~800 nm (Fig. S1B†). The TEM and SEM in Fig. S2C† showed the morphologies of nanoAu/MCN. The nanoAu was effectually grown on the MCN. The size of nanoAu which was synthesized by the chemical process was uneven from 6 nm to 750 nm. In the TEM, some small nanoAu, *e.g.* diameter of ~11 nm, could enter into the pores of MCN, but the big ones distributed on the surface.

The curve of MCN (ESI,† Fig. S2A) showed a representative type IV structure curve with IUPAC classification,[31] and the $N_2$ adsorption–desorption isotherms of MCN revealed typical hysteresis loops in the $P/P_0$ range 0.5 to 0.9, demonstrating the uniform mesopore sizes of MCN. The pore-size distribution curve (ESI,† Fig. S3B) showed that the surface area of

 

MCN tested by the Brunauer–Emmett–Teller (BET) method was 1200.4 $m^2$ $g^{-1}$, and the pore size distribution curve exhibited a diameter of 4.3 nm.

Meanwhile, the cyclic voltammetry (CV) was performed for demonstrating the performance of the modified electrode in PBS (pH 7.4) containing 5.0 mM $[Fe(CN)_6]^{3-/4-}$ (1 : 1) and 10 mM KCl at a scan rate of 50 mV $s^{-1}$. A pair of obvious redox peaks (ESI,† Fig. S3), which were produced by the bare GCE exhibited the anodic and cathodic peak potentials of 0.28 V and 0.14 V, respectively. The anodic and cathodic peak currents sharply increased when MCN and EAu were coated on the GCE in sequence. But the modification of the DNA on the EAu/MCN/GCE resulted in a small decline of the redox peak current. These CV curves demonstrated that the electrode modification was feasible and had a good current response capability.

### 3.3. Optimization of detection conditions

Three replicates were used in all parameter analysis. In order to obtain an acceptable signal response, a series of optimization experiments were carried out by differential pulse voltammetry (DPV). Two kinds of factors were included: (1) the electrodeposition time of EAu, reaction time with $Pb^{2+}$ ions, the effect of pH conditions, the temperature effect on the S1 cleavage efficiency; (2) the MB adsorption conditions of nanoAu/MCN.

As shown in ESI,† Fig. S4A, the electrical signal reached the maximum when the electrodeposition time was 60 s. The increased amount of EAu could provide binding sites for DNA sharply at a time of 50 s. With the purpose to enhance the sensitivity of the sensor, more EAu could be beneficial to mediate the electron transfer and provide more sites for DNA probes combination. Meanwhile, the sensor performance was weakened with too much EAu covering the modified electrode surface when the electrodeposition time was over 60 s. With the growth in reaction time with $Pb^{2+}$, the current response had an ascent and reached a maximum in the reaction time of 30 min. Therefore, 30 min was chosen as the optimized reaction time with $Pb^{2+}$ (ESI,† Fig. S4B). The pH test was conducted in the range from 5.5 to 9.0 (ESI,† Fig. S4C). The DNA double helix was denatured and split into ssDNAs with the value of pH ranging from 8.11 to 12. The low value of pH can make the phosphodiester backbone of DNA hydrolyze, further reducing the DNA to nucleotides and nucleosides.[32] The current response came to a maximum at pH 8.0, and pH 8.0 was the optimal pH condition. The temperature effect was tested between 20 °C, 30 °C, 37 °C, 46 °C and 60 °C (ESI,† Fig. S4D). The substrate S1 was cleaved by enzyme S2 because of the critical melting temperature of 46 °C of the DNA. As the temperature decreased below the melting temperature, the current response was enhanced significantly. The electric signal reached a maximum at 46 °C. Therefore, 46 °C was chosen for the optimized temperature.

MB was adsorbed by nanoAu/MCN and became a part of the signal amplifier. There were several factors which could impact the performance of the signal amplifier, such as pH, interference by coexisting ions, temperature and the reaction time. The solid and liquid were separated with centrifugation for nanoAu/MCN and an ultraviolet spectrophotometer was utilized for the absorbance (Abs) test. The Abs of 5 mg $L^{-1}$ MB was 1.003. The value of pH was adjusted to 5.0, 5.5, 6.0, 6.5, 7.0, 7.5, 8.0, 8.5 and 9.0 to measure the supernatant's Abs after centrifugation. 0.1 M HCl or NaOH was used to adjust the solution pH in the test. The Abs had a decreasing trend at the value of pH ranging from 5.0 to 8.0, and Abs reached the minimum at 8.0 and then increased (ESI,† Fig. S5A). That result indicated that the amount of MB immobilized on nanoAu/MCN was maximal at the value of pH 8.0. The amount of MB decreased in an acidic environment. $H^+$ could competitively adsorb with the cationic group of MB on the active unit.[33] With the increase of pH value, the adsorption of MB was improved. 3 mg nanoAu/MCN was dissolved in 50 mL 0.2 mM MB which contained the same concentrations of $Na^+$, $K^+$, $NH^{4+}$, $Cl^-$, $NO^{3-}$, $SO_4^{2-}$ and $PO_4^{3-}$. There was not a significant effect on the adsorption of MB (ESI,† Fig. S5B). The reaction temperature, such as 4 °C, 10 °C, 15 °C, 20 °C, 25 °C, 30 °C, 35 °C and 40 °C, was tested to make sure that MB adsorption came to the maximum. We could conclude that 30 °C was the best temperature for MB adsorption from the image in ESI,† Fig. S5C. In order to

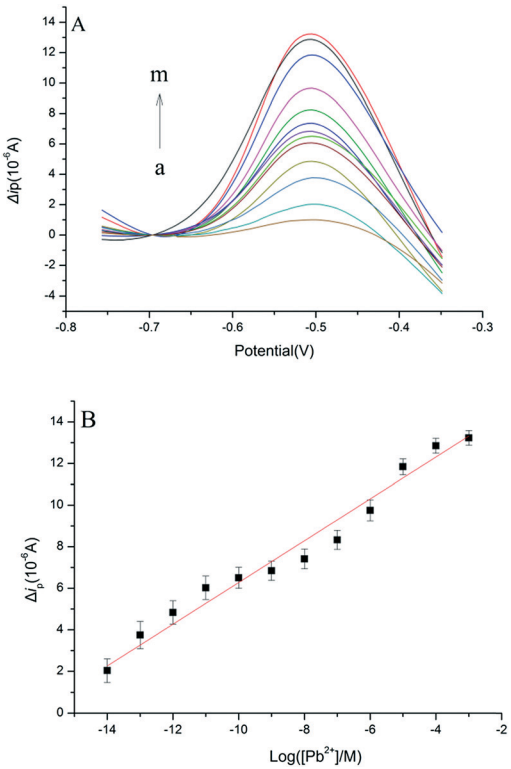


**Fig. 1** The DPV responses of MB for $Pb^{2+}$ detection (A). Concentration of $Pb^{2+}$ from a to m: 0 M, $1.0 \times 10^{-14}$ M, $1.0 \times 10^{-13}$ M, $1.0 \times 10^{-12}$ M, $1.0 \times 10^{-11}$ M, $1.0 \times 10^{-10}$ M, $1.0 \times 10^{-9}$ M, $1.0 \times 10^{-8}$ M, $1.0 \times 10^{-7}$ M, $1.0 \times 10^{-6}$ M, $1.0 \times 10^{-5}$ M, $1.0 \times 10^{-4}$ M and $1.0 \times 10^{-3}$ M. The linear relationship between the DPV peak current change and the logarithm of the concentration of $Pb^{2+}$ (B). The bars represent the standard deviations of the mean values ($n$ = 3).

demonstrate the adsorption influence of time, 5 min, 10 min, 20 min, 30 min, 60 min, 90 min, 120 min, 180 min, 240 min and 300 min were tested. The adsorption had an increasing tendency up to 60 min, and at the time of 90 min, there was no sign of improvement. 90 min was the MB adsorption time (ESI,† Fig. S5D).

### 3.4. Detectability of $Pb^{2+}$

The double helix which was formed by S1 and S2 was cleaved in the presence of $Pb^{2+}$ and the S1 was broken into two fragments at the scissile *rA*. S1 divided into NS1′ and SS1′, and the two fragments were still combined on the MB/nanoAu/MCN signal carrier. NS1′ could hybridize with S3 and connected the MB/nanoAu/MCN signal amplifier to the EAu/MCN modified electrode. Then the current response could be recognized by the electrochemistry system.

The current response of the sensor produced by the distance change between the redox species and the surface of the electrode was detected by the electrochemistry system in general. In the DNA electrochemical sensor, the target probe induced other strands' hybridization to achieve the aim of enhancing the signal. In order to test the performance of the $Pb^{2+}$ sensor, various concentrations of $Pb^{2+}$ were detected by DPV. As shown in Fig. 1A, the current response was quite weak in the solution without $Pb^{2+}$. With the increasing of $Pb^{2+}$ concentration, the signal gradually became stronger. The detection concentrations ranged from $1.0 \times 10^{-3}$ M to $1.0 \times 10^{-14}$ M with the following regression equation:

$$Y = -(16.332 \pm 0.421) - (1.005 \pm 0.052)\chi \quad (1)$$

$Y$ is the peak current difference (A), $\chi$ is the logarithm of $Pb^{2+}$ concentration. In Fig. 1B, the change of peak current linear regression coefficient result was 0.971, and the detection limit was $1.0 \times 10^{-14}$ M. Table 1 shows that the sensitivity of the DNA electrochemical sensor was superior to other methods for detecting $Pb^{2+}$ using fluorescence, colorimetry, surface enhanced Raman spectroscopy (SERS), electrochemiluminescence (ECL) and chips.[34–41] The proposed sensor could completely meet the requirement of water-quality monitoring.

### 3.5. Reproducibility, stability and selectivity

Reproducibility was tested by detecting $Pb^{2+}$ with three different concentrations: $1.0 \times 10^{-8}$ M, $1.0 \times 10^{-10}$ M and $1.0 \times 10^{-12}$ M, using the same process for fabricating the sensor. Stability was determined by successive measurements in triplicate, the maximum relative standard deviation was 4.73%, and those tests were able to ensure the precision of the $Pb^{2+}$ sensor. With the purpose of investigating the selectivity of the $Pb^{2+}$ sensor, several environmentally relevant metal ions were detected, such as $K^+$, $Ca^{2+}$, $Mg^{2+}$, $Al^{3+}$, $Zn^{2+}$, $Fe^{3+}$, $Cu^{2+}$, $Hg^+$, $Cd^{2+}$, $Cr^{2+}$ and $Ni^+$. As seen in Fig. 2, all ions ($1.0 \times 10^{-12}$ M) except $Pb^{2+}$ resulted in little change in the signal response. Apparently, the potential interference of these metal ions with the sensor is minimal.

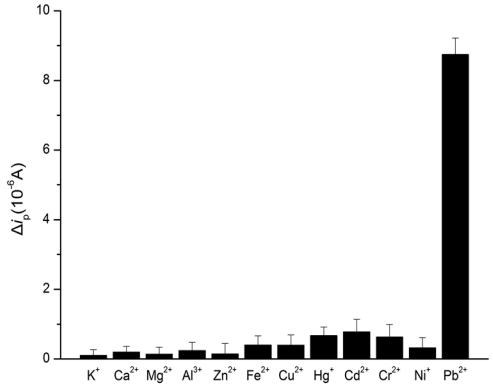


Fig. 2 Selectivity of the electrochemical sensor for $Pb^{2+}$. The concentration of $Pb^{2+}$ and other metal ions was kept at $1.0 \times 10^{-12}$ M. The bars represent the standard deviations of the mean values ($n$ = 3).

### 3.6. Analysis of environmental samples

In order to demonstrate the application of the proposed method, tap water, Xiangjiang River water and the spring water of Yuelu Mountain samples spiked with a fixed amount of $Pb^{2+}$ were tested with the proposed sensor for the sake of demonstrating the performance. All the samples were pretreated in the same way by filtering through a 0.2 μm membrane before detection. The tap water sample was collected after discharging for about 30 min and boiling for 10 min to remove chlorine. As the results in Table 2 show, the average recoveries ranged from 99.2% to 101.8% for three tests, demonstrating the good accuracy of the proposed method for $Pb^{2+}$ detection in the samples.

## 4. Conclusions

A DNA electrochemical sensor for $Pb^{2+}$ determination based on nanomaterials and target-induced electronic switching

Table 1 Determination of $Pb^{2+}$ in water samples

| Target | Detection limit | Detection method | Ref. |
|---|---|---|---|
| $Pb^{2+}$ | $1.2 \times 10^{-11}$ M | DNA electrochemical sensor | 34 |
| | $1.0 \times 10^{-11}$ M | DNA electrochemical sensor | 35 |
| | $9.0 \times 10^{-11}$ M | Fluorescence | 36 |
| | $3.0 \times 10^{-10}$ M | Fluorescence | 37 |
| | $2.0 \times 10^{-8}$ M | Colorimetry | 38 |
| | $5.0 \times 10^{-12}$ M | SERS | 39 |
| | $3.5 \times 10^{-13}$ M | ECL | 40 |
| | $8.9 \times 10^{-12}$ M | Chip | 41 |
| | $1.2 \times 10^{-14}$ M | DNA electrochemical sensor | This work |

Table 2 Determination of $Pb^{2+}$ in water samples

| Sample | Original[a] (nM) | Spiked (nM) | Found[b] (nM) | Recovery (%) |
|---|---|---|---|---|
| Tap water | 0 | 20 | 20.25 | 101.8 |
| Spring water | 28.75 | 20 | 48.69 | 99.2 |
| River water | 26.54 | 20 | 46.69 | 100.3 |

[a] Mean of three measurements. [b] Mean of three measurements.

was developed with a detection limit of $1.0 \times 10^{-14}$ M. The EAu and MCN were assembled on the surface of a GCE, capable of providing a huge specific surface area and pore volume, high electrical conductivity, and favorable biocompatibility for DNA combination. The signal amplifier fabricated with NS1′/MB/nanoAu/MCN could enhance the current response and the sensitivity of the proposed sensor. The MB/nanoAu/MCN could be connected to the modified electrode in the presence of $Pb^{2+}$, and was able to induce the signal response significantly. The secondary structure of the 8–17 DNAzyme possesses the ability to promote the selectivity of $Pb^{2+}$ detection. The DNA electrochemical sensor has exhibited excellent selectivity and can be applied in water samples. In conclusion, the proposed $Pb^{2+}$ sensor exhibits prominent performance and deserves to be promoted for other metal ions' detection.

## Acknowledgements

This work was supported by the National Natural Science Foundation of China (No. 51521006, 51222805, 51579096, 51508175, 51378190), the Key Technology R&D Program of Hunan Province, China (2015SK2001-1), the National Program for Support of Top-Notch Young Professionals of China (2012) and the International S&T Cooperation Program of China (2015DFG92750).

## References

1 H. N. Kim, W. X. Ren, J. S. Kim and J. Y. Yoon, *Chem. Soc. Rev.*, 2012, **41**, 3210–3244.
2 G. M. Zeng, M. Chen and Z. T. Zeng, *Nature*, 2013, **499**, 154.
3 G. M. Zeng, M. Chen and Z. T. Zeng, *Science*, 2013, **340**, 1403.
4 K. P. Carter, A. M. Young and A. E. Palmer, *Chem. Rev.*, 2014, **114**, 4564–4601.
5 F. Perreault, A. F. de Fonseca and M. Elimelech, *Chem. Soc. Rev.*, 2015, **44**, 5861–5896.
6 S. Yavuz, A. Erkal, I. F. Kariper, A. O. Solak, S. Jeon, İ. E. Mülazımoğlu and Z. Üstündağ, *Food. Anal. Methods*, 2016, **9**, 322–331.
7 H. Xu, S. Xu, Y. Zhu, W. Xu, P. Zhou, C. Zhou, B. Dong and H. Song, *Nanoscale*, 2014, **6**, 12573–12579.
8 M. Y. Naseri, M. R. M. Hosseini, Y. Assadi and A. Kiani, *Talanta*, 2008, **75**, 56–62.
9 G. Yang, Q. Hu, Z. Huang and J. Yin, *J. Braz. Chem. Soc.*, 2005, **16**, 1154–1159.
10 M. Wang, W. Feng, J. Shi, F. Zhang, B. Wang, M. Zhu, B. Li, Y. Zhao and Z. Chai, *Talanta*, 2007, **71**, 2034–2039.
11 Y. Wu, F. Huang and Y. Lin, *ACS Appl. Mater. Interfaces*, 2013, **5**, 1503–1509.
12 J. Zhang, Y. Tang, L. Teng, M. Lu and D. Tang, *Biosens. Bioelectron.*, 2015, **68**, 232–238.
13 Y. Xiao, A. A. Rowe and K. W. Plaxco, *J. Am. Chem. Soc.*, 2007, **129**, 262–263.
14 L. Li, J. Feng, Y. Fan and B. Tang, *Anal. Chem.*, 2015, **87**, 4829–4835.
15 Y. Lu, *Chem. – Eur. J.*, 2002, **8**, 4588.
16 H. K. Kim, J. Liu, J. Li, N. Nagraj, M. Li, C. M. B. Pavot and Y. Lu, *J. Am. Chem. Soc.*, 2007, **129**, 6896–6902.
17 J. Li and Y. Lu, *J. Am. Chem. Soc.*, 2000, **122**, 10466–10467.
18 W. Song, J. Li, Q. Li, W. Ding and X. Yang, *Anal. Biochem.*, 2015, **471**, 17–22.
19 M. Khairy, S. A. El-Safty, M. A. Shenashen and E. A. Elshehy, *Nanoscale*, 2013, **5**, 7920–7927.
20 Y. Zhang, G. M. Zeng, L. Tang, Y. P. Li, Z. M. Chen and G. H. Huang, *RSC Adv.*, 2014, **4**, 18485.
21 Y. Zhang, G. M. Zeng, L. Tang, Y. P. Li, L. J. Chen, Y. Pang, Z. Li, C. L. Feng and G. H. Huang, *Analyst*, 2011, **136**, 4202.
22 Y. Zhu, G. M. Zeng, Y. Zhang, L. Tang, J. Chen, M. Cheng, L. H. Zhang, L. He, Y. Guo, X. X. He, M. Y. Lai and Y. B. He, *Analyst*, 2014, **139**, 5014.
23 Y. Zhang, G. M. Zeng, L. Tang, J. Chen, Y. Zhu, X. X. He and Y. B. He, *Anal. Chem.*, 2015, **87**, 989–996.
24 Z. S. Qian, X. Y. Shan, L. J. Chai, J. R. Chen and H. Feng, *Biosens. Bioelectron.*, 2015, **68**, 225–231.
25 Y. Y. Zhou, L. Tang, G. M. Zeng, J. Chen, Y. Cai, Y. Zhang, G. D. Yang, Y. Liu, C. Zhang and W. W. Tang, *Biosens. Bioelectron.*, 2014, **61**, 519–525.
26 L. Jia, H. Wang, D. Dhawale, C. Anand, M. A. Wahab, Q. Ji, K. Arigab and A. Vinu, *Chem. Commun.*, 2014, **50**, 5976–5979.
27 Y. Shi, Y. Wan and D. Zhao, *Chem. Soc. Rev.*, 2011, **40**, 3854–3878.
28 A. Yu, Z. Liang, J. Cho and F. Caruso, *Nano Lett.*, 2003, **3**, 1203–1207.
29 P. Wu, K. Hwang, T. Lan and Y. Lu, *J. Am. Chem. Soc.*, 2013, **135**, 5254–5257.
30 Y. Y. Zhou, L. Tang, G. M. Zeng, J. Chen, J. J. Wang, C. Fan, G. D. Yang, Y. Zhang and X. Xie, *Biosens. Bioelectron.*, 2015, **65**, 382–389.
31 X. Y. Tao, X. R. Chen, Y. Xia, H. Huang, Y. Q. Gan, R. Wu, F. Chen and W. K. Zhang, *J. Mater. Chem. A*, 2013, **1**, 3295–3301.
32 J. Liu and Y. Lu, *Chem. Mater.*, 2004, **16**, 3231–3238.
33 M. Doğan, M. Alkan, A. Türkyilmaz and Y. Özdemir, *J. Hazard. Mater.*, 2004, **104**, 141–148.
34 C. Zhang, C. Lai, G. M. Zeng, D. L. Huang, L. Tang, C. P. Yang, Y. Y. Zhou, L. Qin and M. Cheng, *Biosens. Bioelectron.*, 2016, **81**, 61–67.
35 Z. Yu, W. Zhou, J. Han, Y. C. Li, Z. Fan and X. H. Li, *Anal. Chem.*, 2016, **88**, 9375–9380.
36 M. Li, X. J. Zhou, S. W. Guo and N. Q. Wu, *Biosens. Bioelectron.*, 2013, **43**, 69–74.
37 X. H. Zhao, R. M. Kong, X. B. Zhang, H. M. Meng, W. N. Liu, W. H. Tan, G. L. Shen and R. Q. Yu, *Anal. Chem.*, 2011, **83**, 5062–5066.
38 J. Zhu, Y.-Q. Yu, J.-J. Lia and J.-W. Zhao, *RSC Adv.*, 2016, **6**, 25611–25619.
39 G. Pelossof, R. Tel-Vered and I. Willner, *Anal. Chem.*, 2012, **84**, 3703–3709.
40 Y. M. Lei, W. X. Huang, M. Zhao, Y. Q. Chai, R. Yuan and Y. Zhuo, *Anal. Chem.*, 2015, **87**, 7787–7794.
41 Y. Shi, H. Y. Wang, X. X. Jiang, B. Sun, B. Song, Y. Y. Su and Y. He, *Anal. Chem.*, 2016, **88**, 3723–3729.